Probing Postmeasurement Entanglement without Postselection

Samuel J. Garratt[1,*] and Ehud Altman[1,2]

[1] *Department of Physics, University of California, Berkeley, California 94720, USA*

[2] *Materials Science Division, Lawrence Berkeley National Laboratory, Berkeley, California 94720, USA*

(Received 17 October 2023; revised 11 May 2024; accepted 13 June 2024; published 18 July 2024)

We study the problem of observing quantum collective phenomena emerging from large numbers of measurements. These phenomena are difficult to observe in conventional experiments because, in order to distinguish the effects of measurement from dephasing, it is necessary to postselect on sets of measurement outcomes with Born probabilities that are exponentially small in the number of measurements performed. An unconventional approach, which avoids this exponential "postselection problem", is to construct cross-correlations between experimental data and the results of simulations on classical computers. However, these cross-correlations generally have no definite relation to physical quantities. We first show how to incorporate classical shadows into this framework, thereby allowing for the construction of quantum information-theoretic cross-correlations. We then identify cross-correlations that both upper and lower bound the measurement-averaged von Neumann entanglement entropy, as well as cross-correlations that lower bound the measurement-averaged purity and entanglement negativity. These bounds show that experiments can be performed to constrain postmeasurement entanglement without the need for postselection. To illustrate our technique, we consider how it could be used to observe the measurement-induced entanglement transition in Haar-random quantum circuits. We use exact numerical calculations as proxies for quantum simulations and, to highlight the fundamental limitations of classical memory, we construct cross-correlations with tensor-network calculations at finite bond dimension. Our results reveal a signature of measurement-induced criticality that can be observed using a quantum simulator in polynomial time and with polynomial classical memory.

DOI: 10.1103/PRXQuantum.5.030311

I. INTRODUCTION

Local measurements allow for the protection and control of quantum correlations and are essential for error-corrected quantum computation [1]. This aim has motivated the development of local readout techniques in quantum simulation platforms from trapped-ion [2] and neutral-atom arrays [3] to superconducting quantum processors [4]. New questions also arise in many-body quantum mechanics, in particular about the effects of many measurements on entangled quantum states. Examples of phenomena arising in this setting are the measurement-induced entanglement transitions in quantum circuits [5–8], as well as the creation [9–17] and restructuring [18–23] of entangled states through measurement.

Experiments studying the effects of many measurements must, however, be conducted in a fundamentally different way. This is because, to characterize a quantum state in experiment, we must prepare and measure it more than once. If the preparation of this state involves measurements, we are then forced to postselect for sets of outcomes with probabilities that are exponentially small in the number of measurements performed, and hence the time required is exponentially large [24]. Moreover, averaging over runs of an experiment has the effect of converting measurements into dephasing events, obscuring structures in the ensemble of postmeasurement states.

Two different strategies have emerged for avoiding this "postselection problem," each involving a simulation on a classical computer (a "classical simulation"). One possibility is to use experimental measurement outcomes as input to the calculation of a unitary operation that decodes quantum information [25–27]; this protocol is analogous to the decoding step in quantum teleportation [28]. The second strategy, which is the focus of this work, is to calculate cross-correlations between the results of experiments and classical simulations of the system [14,18,29–31]. This strategy has the advantage that the effects of

*Contact author: sjgarratt@berkeley.edu

measurements can be inferred in classical postprocessing and hence the duration of the classical simulation is not limited by experimental decoherence time scales. The idea is closely related to cross-entropy benchmarking, studied in the contexts of random circuit sampling [32] and the measurement-induced entanglement transition [33], with the important difference that the cross-correlations of Refs. [14,18,29,31] are designed to probe properties of postmeasurement quantum states rather than statistical properties of the measurement record.

Ultimately, however, the aim of experiment should be to extract information intrinsic to the system. The problem with constructing probes that depend on classical simulations, based on either decoding or cross-correlation, is that the results depend sensitively on how we choose to model the system. Given the apparent necessity of involving a classical simulation, it is natural to ask whether it is even possible to probe intrinsic properties of postmeasurement quantum states without postselection.

In this work, we show that cross-correlations between experimental data and classical simulations can be used to bound model-independent properties of postmeasurement states. Our cross-correlations are inspired by classical shadows [34,35]; shadows of a density matrix have the property that, when suitably averaged, they reproduce the density matrix, but in the regime in which there is a postselection problem we will not be able to perform this average. Nonetheless, we will show that cross-correlations taking shadows of postmeasurement states as input can be used to construct an estimate for the measurement-averaged entanglement entropy (see Fig. 1). By identifying this estimate as a contribution to an averaged quantum relative entropy, which is non-negative, we arrive at a resource-efficient upper bound on the true measurement-averaged entanglement entropy. This bound becomes an equality for a perfect classical simulation. Using the monotonicity of the quantum relative entropy, we also construct an upper bound on the conditional entropy [1]. Recasting this as a lower bound on the entanglement entropy, we identify physical settings where the entanglement can be determined to within a threshold set by the accuracy of the classical simulation.

While a quantum simulation can represent a highly entangled many-body state, the classical memory required for this is in general exponentially large in the entanglement entropy. This difference between quantum and classical memory imposes a fundamental obstacle to schemes involving classical simulations. To investigate the effects of a constrained classical memory we consider an application of our approach in the context of the measurement-induced entanglement transition [5–8]. In place of a quantum simulation, we use exact numerics to study the dynamics of one-dimensional chains of $L \leq 24$ qubits and we cross-correlate the results with matrix-product state (MPS) simulations at finite bond dimension χ. The MPS

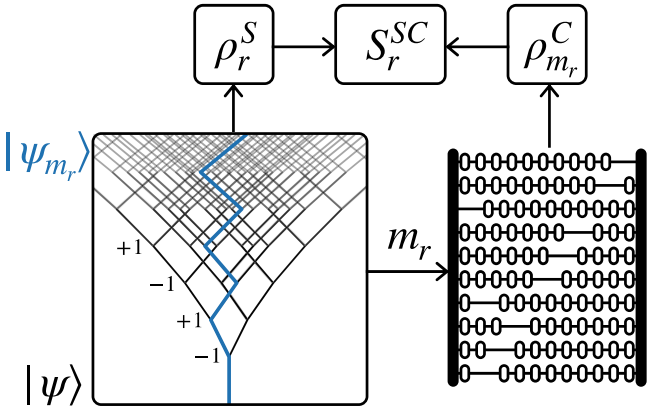

FIG. 1. An illustration of the protocol for a single run r. The branching process on the left represents an experiment involving measurements that takes the system from initial state $|\psi\rangle$ to postmeasurement state $|\psi_{m_r}\rangle$, where m_r is the set of M measurement outcomes observed in run r (here indicated by ± 1). In each run, one extracts a single shadow ρ_r^S of a subsystem density matrix ρ_{m_r}. The outcomes m_r are used as input to a calculation on a classical computer (represented by the abacus) and this calculation returns an estimate $\rho_{m_r}^C$ for the density matrix ρ_{m_r}. Finally, one constructs the object $S_r^{SC} = -\mathrm{Tr}[\rho_r^S \log \rho_{m_r}^C]$. Averaging S_r^{SC} over runs of the experiment generates an upper bound on the measurement-averaged entanglement entropy of the density matrices ρ_{m_r}.

representation only occupies classical memory $\sim L\chi^2$, to be contrasted with $\sim 2^L$ for a generic many-body quantum state. Increasing χ improves the simulation, causing our upper bound on the measurement-averaged entanglement to become more restrictive. In the vicinity of measurement-induced criticality, we show numerically that the separation between the upper bound and the exact value decays exponentially as $\sim e^{-\chi/\chi^{QC}(L)}$ with increasing χ, and that the decay constant $\chi^{QC}(L)$ grows as a power of L. This result suggests that the generic measurement-induced entanglement transition can be observed in experiment with computational resources that scale only polynomially with system size.

The fact that the measurement-averaged entanglement entropy can be bounded without postselection has more general implications. For example, it opens the door to experiments on deep thermalization [36–42], measurement-induced teleportation [43–46], and measurement-altered criticality [18–23]. Moreover, by converting the postselection problem into a variational problem, our work suggests a way to improve classical simulations using experimental data.

It is important to separate our approach from adaptive schemes. If individual measurement outcomes are used as input to local unitary feedback operations, nontrivial correlations [10,12,15–17,47] and dynamics [48–52] may be probed without postselection, i.e., through the density

matrix averaged over runs of the experiment. With or without feedback, such an average washes out the features in the ensemble of postmeasurement states that are of interest here (such as measurement-induced entanglement transitions [53–56]). A key physical difference is that averaging over the outcome of a measurement converts it into a quantum channel and, although local measurements can have nonlocal effects on entangled states, local quantum channels cannot.

This paper is organized as follows. In Sec. II we outline the origin of the postselection problem and in Sec. III we describe quantum-classical cross-correlations. There, we also provide a first example of how these cross-correlations can be used to bound physical quantities. In Sec. IV, we discuss shadows, use them to construct matrix-valued cross-correlations, and then derive a bound on the measurement-averaged purity. Following this, in Sec. V we introduce resource-efficient bounds on the measurement-averaged von Neumann entanglement entropy and in Sec. VI we discuss their statistical fluctuations. Section VII addresses the measurement-induced entanglement transition and in Sec. VIII we discuss the connection between our work and Ref. [25]. In Sec. IX we then present a bound on the measurement-averaged entanglement negativity. We summarize our results and offer an outlook in Sec. X.

II. POSTSELECTION PROBLEM

Here, we discuss the postselection problem. We consider experiments involving $M \gg 1$ measurements, having sets of outcomes m, which create postmeasurement quantum states that depend on m. For example, if we have a system of L qubits in a random pure state and we measure the Pauli-Z operator on $M = L - 2$ of the qubits, finding outcomes m, we are left with a random pure state on the two unmeasured qubits. We could then ask how to characterize the postmeasurement density matrix ρ_m of one of these two qubits. More generally, the postmeasurement density matrices ρ_m discussed in this work will be taken to describe states of a number of qubits of order unity.

To characterize the density matrix ρ_m, we must measure an observable, and this returns one of the eigenvalues of the observable. To determine the postmeasurement expectation value, on the other hand, we must prepare ρ_m multiple times. The problem is that the probability P_m of observing m is, in general, exponentially small in M. If we repeat the experiment a finite number of times R, then for large M we typically have $P_m R \ll 1$ and hence we expect to find each m no more than once. Therefore, we cannot characterize the ensemble of ρ_m in a conventional way. Throughout this work, we will label the runs of the experiment $r = 0, \ldots, (R-1)$ and the corresponding sets of outcomes $m_r = (m_{r,0}, \ldots, m_{r,M-1})$. "Monte Carlo" averages over $R \gg 1$ runs of the experiment will be denoted by $\mathbb{E}_r[\cdots]$, while averages over the ensemble of all outcomes (weighted by their respective Born probabilities P_m) will be denoted $\mathbb{E}_m[\cdots]$.

Suppose that in each run r of the experiment, we probe a postmeasurement density matrix ρ_{m_r} by measuring a Pauli matrix Z. This "probe" measurement should be distinguished from the M "preparation" measurements which generate the ensemble of states that we hope to characterize. The result of the probe measurement is $z_r = \pm 1$, corresponding to state $|z_r\rangle$, but if we average z_r over runs we find only a property of the "dephased" density matrix $\mathbb{E}_m[\rho_m] = \sum_m P_m \rho_m$,

$$\mathbb{E}_r[z_r] = \mathbb{E}_m[\langle Z\rangle_m] = \mathrm{Tr}\left[\mathbb{E}_m[\rho_m] Z\right], \tag{1}$$

where $\langle Z\rangle_m = \mathrm{Tr}[\rho_m Z]$. Here, the average over runs, which occurs in classical postprocessing, has the effect of converting our measurements into dephasing. This is because we have chosen to average an object that is linear in the postmeasurement density matrices. Averages that distinguish the effects of measurement from dephasing are nonlinear in the postmeasurement density matrices but such averages cannot be determined without postselection. For example, there is no way to construct an average that converges to $\mathbb{E}_m[\langle Z\rangle_m^2]$ if we have only one eigenvalue z_r for each observed outcome m_r.

Here, we have described the origin of the postselection problem, which arises for large M. The effects of measurements are physically distinct from dephasing but standard averages over results of our experiment are blind to this difference. Our limitation is that we have access only to sets of outcomes m_r and the results of our "probe" measurements, such as z_r above. In Sec. III, we describe how to use this information to detect structure in the ensemble of postmeasurement density matrices.

III. CROSS-CORRELATIONS

To understand quantum-classical cross-correlations, let us return to the above example of preparing postmeasurement density matrices ρ_{m_r} and trying to characterize them by measuring Z. Our discussion in this section largely follows Ref. [18]. It will be convenient to write the observed eigenvalue of Z as

$$z_r = \langle Z\rangle_{m_r} + [z_r - \langle Z\rangle_{m_r}]. \tag{2}$$

Averaging over runs of the experiment washes out the random fluctuations $[z_r - \langle Z\rangle_{m_r}]$ around the mean $\langle Z\rangle_{m_r}$. The problem is that, through this average, we have also lost information on the variations of $\langle Z\rangle_{m_r}$ across different runs. By cross-correlating the results z_r of our experiment with numbers w_{m_r} that depend on the outcomes m_r but not on z_r,

we can preserve this information:

$$\mathbb{E}_r[w_{m_r} z_r] = \mathbb{E}_m[w_m \langle Z\rangle_m]. \tag{3}$$

There is a lot of freedom in how the weights w_m are chosen. One basic requirement is that w_m depends on m, since otherwise Eq. (3) reduces to Eq. (1). Another is that the ratio of the variance and squared mean of $w_{m_r} z_r$ should grow no faster than polynomially with M, and this requirement rules out $w_{m_r} = \delta_{m_r m}$, which corresponds to postselecting for outcomes m.

With a suitable choice of w_m, we should be able to learn something about the ensemble of ρ_m. In Ref. [18], we advocated for w_m equal to an estimate for the postmeasurement expectation value of an observable, e.g., $w_m = \langle Z\rangle^C_m$. In principle, this estimate is determined via a calculation on a classical computer, which takes the experimental measurement outcomes m as input. The operator used to construct w_m need not be the same as the operator one measures in experiment: the authors of Refs. [29,31] chose w_m to be equal to the sign of the expectation value $\langle Z\rangle^C_m$.

By choosing such a w_m, the experimentally accessible probe of the measured quantum system becomes a cross-correlation between experiment and theory. With $w_m = \langle Z\rangle^C_m$, we have

$$\mathbb{E}_r[\langle Z\rangle^C_{m_r} z_r] = \mathbb{E}_m[\langle Z\rangle^C_m \langle Z\rangle_m]. \tag{4}$$

This quantum-classical cross-correlation can then be compared with the result of the simulation,

$$\mathbb{E}_r[\langle Z\rangle^C_{m_r} \langle Z\rangle^C_{m_r}] = \mathbb{E}_m[\langle Z\rangle^C_m \langle Z\rangle^C_m], \tag{5}$$

which we refer to as the "classical-classical" object. Agreement between quantum-classical and classical-classical quantities allows one to verify that the quantum simulation behaves, at least at an averaged level, in the same way as the classical simulation. Unfortunately, such a comparison does not yet provide us with information about intrinsic properties of the quantum system, such as the "quantum-quantum" object $\mathbb{E}_m[\langle Z\rangle_m \langle Z\rangle_m]$.

However, we can take a step beyond Refs. [18,29,31] using the trivial inequality $\mathbb{E}_r[(\langle Z\rangle_{m_r} - \langle Z\rangle^C_{m_r})^2] \geq 0$, which can be rewritten using Eq. (4) as

$$\mathbb{E}_m[\langle Z\rangle^2_m] \geq \mathbb{E}_r\left[2 z_r \langle Z\rangle^C_{m_r} - \langle Z\rangle^C_{m_r} \langle Z\rangle^C_{m_r}\right]. \tag{6}$$

Equation (6) shows us that, although we cannot determine $\mathbb{E}_m[\langle Z\rangle^2_m]$ directly, we can bound it using cross-correlations between classical and quantum simulations. Before deriving bounds on the measurement-averaged entanglement entropy, we generalize the above scheme using classical shadows.

IV. INCORPORATING SHADOWS

It will be useful to first describe shadows [35] in their simplest incarnation for a single qubit. If one can prepare a density matrix ρ multiple times, in each run r of the experiment one applies a random unitary U_r and then measures Z, finding a result z_r. The shadow $\rho^S_r = \rho^S(z_r, U_r)$ is defined as the matrix satisfying

$$\mathbb{E}_r[\rho^S_r] = \sum_{U,z} P_U P_{z\,|\,U} \rho^S(z, U) = \rho, \tag{7}$$

where P_U is the probability that we have chosen the unitary U and $P_{z\,|\,U} = \langle z|U\rho U^{-1}|z\rangle$ is the Born probability for finding result z given that we have acted with U. If the set of U forms a 2-design for the Haar ensemble of single-qubit unitary operators, we should choose

$$\rho^S_r = 3U^{-1}_r |z_r\rangle \langle z_r| U_r - \mathbb{1}, \tag{8}$$

where $Z|z_r\rangle = z_r |z_r\rangle$. Note that ρ^S_r is not a valid density matrix, since its eigenvalues are not all positive. It is nevertheless the case that its average over z and U is the density matrix ρ. This behavior can be verified using the first two moments of the Haar distribution over the unitary group. Generalizing Eq. (8) to multiple qubits is straightforward [34]: one possibility is to construct N-qubit shadows as the tensor products of N objects with the structure $3U^{-1}|z\rangle\langle z|U - \mathbb{1}$.

Shadow tomography requires that ρ can be prepared multiple times. In our case, we cannot efficiently prepare the postmeasurement density matrices ρ_m but, as we now show, we can nevertheless apply some of the ideas above. Suppose that in each run r we prepare a single-qubit density matrix ρ_{m_r}, choose a random unitary U_r, and measure Z, finding a result z_r. The shadow in this run is given by Eq. (8) or, e.g., as a tensor product of these objects if ρ_{m_r} is a density matrix for multiple qubits. Now, we write the matrix analogue of Eq. (2) as

$$\rho^S_r = \rho_{m_r} + [\rho^S_r - \rho_{m_r}] \tag{9}$$

where $[\rho^S_r - \rho_{m_r}]$ is a mean zero fluctuation. Given an m-dependent set of matrices W_m, as in Eq. (3), our average over runs can wash out these fluctuations while preserving information on the ensemble of ρ_m,

$$\mathbb{E}_r[W_{m_r} \rho^S_r] = \sum_m P_m W_m \sum_{U,z} P_U P_{z\,|\,U,m} \rho^S(z, U), \tag{10}$$

where $P_{z\,|\,U,m} = \langle z|U\rho_m U^{-1}|z\rangle$. Provided that the unitary operations used to construct the shadows are sampled independently of m, we can perform the averages over U and z

in this expression, to arrive at

$$\mathbb{E}_r[W_{m_r}\rho_r^S] = \mathbb{E}_m[W_m\rho_m]. \tag{11}$$

This relation will allow us to probe quantum information-theoretic quantities without postselection.

If we choose W_m based on a classical simulation, e.g., setting it equal to the classical estimate for the post-measurement density matrix $W_m = \rho_m^C$, we arrive at a matrix-valued cross-correlation $\mathbb{E}_r[\rho_{m_r}^C\rho_r^S] = \mathbb{E}_m[\rho_m^C\rho_m]$. Taking the trace of this object would give us a "quantum-classical" purity $\mathbb{E}_m[\mathrm{Tr}(\rho_m^C\rho_m)]$. In analogy with Eq. (6), we can use the inequality $\mathrm{Tr}[(\rho_m - \rho_m^C)^2] \geq 0$ to lower bound the measurement-averaged purity:

$$\mathbb{E}_m[\mathrm{Tr}\rho_m^2] \geq \mathbb{E}_r\left[2\mathrm{Tr}(\rho_{m_r}^C\rho_r^S) - \mathrm{Tr}(\rho_{m_r}^C\rho_{m_r}^C)\right]. \tag{12}$$

Equation (12) is our first bound on an entanglement measure. Note that if ρ_m is the density matrix of a finite number of qubits, the variance of the right-hand side of this expression is finite.

V. ENTANGLEMENT ENTROPY

Here, we construct resource-efficient upper [Eq. (20)] and lower [Eq. (25)] bounds on the measurement-averaged von Neumann entanglement entropy. First, it is useful to collect some definitions. The entanglement entropy of ρ_m is defined as

$$S_m = -\mathrm{Tr}[\rho_m \log \rho_m] \tag{13}$$

and our quantum-classical cross-correlation will come from choosing matrix-valued weights

$$W_m = -\log \rho_m^C. \tag{14}$$

Here W_m is the modular Hamiltonian corresponding to ρ_m^C. The estimate W_m could be produced by an approximate classical simulation or another classical model that takes the measurement outcomes as input (e.g., a machine-learning model). In each run r of the experiment, we therefore have a single shadow ρ_r^S as well as the calculated quantity $-\log\rho_{m_r}^C$. From these, we construct

$$S_r^{SC} = -\mathrm{Tr}[\rho_r^S \log \rho_{m_r}^C], \tag{15}$$

which, by Eq. (11), converges to the quantum-classical entanglement entropy upon averaging over experimental runs:

$$\mathbb{E}_r[S_r^{SC}] = \mathbb{E}_m[S_m^{QC}]. \tag{16}$$

Here, we have defined the quantum-classical entanglement entropy

$$S_m^{QC} = -\mathrm{Tr}[\rho_m \log \rho_m^C]. \tag{17}$$

In Sec. VI, we discuss the number of experimental runs required to observe this convergence. It will often be useful to compare $\mathbb{E}_m[S_m^{QC}]$ with the average of the "classical-classical" entanglement entropy,

$$S_m^{CC} = -\mathrm{Tr}[\rho_m^C \log \rho_m^C]. \tag{18}$$

Throughout this work, we reserve the name "entanglement entropy" for the object in Eq. (13), rather than the proxies in Eqs. (15)–(18). It is important to recognize that, without postselection, only S_r^{SC} and S_m^{CC} can be determined for individual outcomes m. It is the average over measurement outcomes that gives us access to $\mathbb{E}_m[S_m^{QC}]$.

A. Upper bound

The upper bound on $\mathbb{E}_m[S_m]$ comes from writing the quantum relative entropy [1] between ρ_m and ρ_m^C as

$$\begin{aligned} D_m &\equiv \mathrm{Tr}[\rho_m(\log\rho_m - \log\rho_m^C)] \\ &= S_m^{QC} - S_m. \end{aligned} \tag{19}$$

From the non-negativity of the quantum relative entropy $D_m \geq 0$, we then have

$$\mathbb{E}_m[S_m] \leq \mathbb{E}_m[S_m^{QC}] = \mathbb{E}_r[S_r^{SC}], \tag{20}$$

where the right-hand side is experimentally accessible. This result shows that although we cannot determine $\mathbb{E}_m[S_m]$ without postselection, we can construct an upper bound using experimental data and classical simulations. Despite its simplicity, Eq. (20) is one of our central results: the fact that it is possible to bound simulation-independent properties of the quantum system using quantum-classical cross-correlations opens the door to new kinds of experiments in quantum simulators. Interestingly, Eq. (20) also reveals that we can use experimental data to optimize our models by minimizing $\mathbb{E}_r[S_r^{SC}]$.

Note that in order for Eq. (20) to hold when some of the eigenvalues of ρ_m^C are zero (e.g., when ρ_m^C is pure), it is necessary to define $-\log\rho_m^C$ as having infinite contributions, i.e., to define the negative logarithms of the zero eigenvalues as infinity. Since we have the freedom to choose ρ_m^C, this is unlikely to be an issue in practice and we can simply impose that all eigenvalues of ρ_m^C be larger than a threshold.

The upper bound in Eq. (20) has a well-known classical analogue. Setting the off-diagonal entries of ρ_m and ρ_m^C to zero, we are left with classical probability distributions along their diagonals and the quantum relative entropy becomes the standard classical relative entropy (also known as Kullback-Leibler divergence). This quantity is also non-negative and we are left with the statement that the logarithmic cross entropy is an upper bound on the classical Shannon entropy.

B. Lower bound

Our lower bound, on the other hand, does not have a useful classical analogue. To arrive at the lower bound on the measurement-averaged entanglement we consider two subregions, A and B. The true postmeasurement density matrices for AB are denoted by $\rho_{AB,m}$ and our classical estimates by $\rho^C_{AB,m}$. It is helpful to first discuss the conditional entropy

$$C_{B\,|\,A,m} = S_{AB,m} - S_{A,m}, \tag{21}$$

where $S_{A,m}$ and $S_{AB,m}$ are postmeasurement entanglement entropies for A and for AB, respectively. For example, $S_{A,m} = -\mathrm{Tr}[\rho_{A,m} \log \rho_{A,m}]$. Note that for classical probability distributions the conditional entropy cannot be negative; this is equivalent to the statement that the Shannon entropy of a system cannot be smaller than the Shannon entropy of one of its subsystems. A negative conditional entropy is therefore an indication that A and B are entangled.

Using the definition given in Eq. (19), we write $S_{A,m} = S^{QC}_{A,m} - D_{A,m}$, as well as the analogous expression for $S_{AB,m}$. Inserting these relations into $C_{B\,|\,A,m}$, we find that

$$C_{B\,|\,A,m} = C^{QC}_{B\,|\,A,m} - D_{AB,m} + D_{A,m} \leq C^{QC}_{B\,|\,A,m}, \tag{22}$$

where we have defined $C^{QC}_{B\,|\,A,m} = S^{QC}_{AB,m} - S^{QC}_{A,m}$. The inequality follows from the monotonicity of the relative entropy $D_{A,m} \leq D_{AB,m}$. In terms of experimentally accessible quantities, we then have

$$\mathbb{E}_m[C_{B\,|\,A,m}] \leq \mathbb{E}_r[C^{SC}_{B\,|\,A,r}], \tag{23}$$

where $C^{SC}_{B\,|\,A,r} = S^{SC}_{AB,r} - S^{SC}_{A,r}$. Therefore, if we find $\mathbb{E}_r[C^{SC}_{B\,|\,A,r}] \leq 0$, we can provide evidence that A and B are entangled on average.

This bound on the conditional entropy can be recast into a lower bound on the entanglement entropy, complementing the upper bound in Eq. (20). Using $C_{B\,|\,A,m} \leq C^{QC}_{B\,|\,A,m}$ and $S_{AB,m} \geq 0$, we have

$$S^{QC}_{A,m} - S^{QC}_{AB,m} \leq S_{A,m}. \tag{24}$$

After averaging, this can be written as

$$\mathbb{E}_r[S^{SC}_{A,r}] - \mathbb{E}_r[S^{SC}_{AB,r}] \leq \mathbb{E}_m[S_{A,m}] \leq \mathbb{E}_r[S^{SC}_{A,r}], \tag{25}$$

where on the right-hand side we have also included the upper bound in Eq. (20) (now with the subregion A of interest specified). The result in Eq. (25) shows that the true measurement-averaged von Neumann entanglement entropy can be both lower and upper bounded without postselection. The upper bound becomes an equality in the limit of a perfect classical simulation. The lower bound, on the other hand, only becomes restrictive for small $\mathbb{E}_r[S^{SC}_{AB,r}]$, but this is possible only if $\mathbb{E}_m[S_{AB,m}]$ is itself small.

Unlike the upper bound in Eq. (20), there is no meaningful classical analogue of the lower bound in Eq. (24). To see this, first note that the lower bound converges to $-\mathbb{E}_m[C^{QC}_{B\,|\,A,m}]$, which is less than or equal to $-\mathbb{E}_m[C_{B\,|\,A,m}]$ from Eq. (23). However, as discussed above, the conditional entropy for a probability distribution is non-negative. For diagonal density matrices the lower bound in Eq. (24) is therefore less than or equal to zero, making it no more restrictive than the fact that Shannon entropies are non-negative. In quantum systems, on the other hand, the entanglement entropy of a system can be smaller than that of one of its subsystems and only in this case (corresponding to negative conditional entropy) is the lower bound in Eq. (24) useful. In summary, although postselection problems can arise in both classical and quantum systems, the resolution represented by the two-sided bound on entanglement in Eq. (25) is specific to the quantum setting.

The existence of the lower bound on postmeasurement entanglement reveals the physical setting in which we can accurately determine the postmeasurement entanglement. If $\mathbb{E}_m[S_{AB,m}] = \delta$, then the separation between the upper and lower bounds is $\mathbb{E}_r[S^{SC}_{AB,r}] \geq \delta$. Therefore, using Eq. (24), we can determine $\mathbb{E}_m[S_{A,m}]$ to an accuracy no better than δ. In closing, we note that regardless of the quality of the classical simulation, the accuracy with which we know the entanglement entropy is itself observable without postselection: if the lower bound in Eq. (25) is positive, then this accuracy is $\mathbb{E}_r[S^{SC}_{AB,r}]$, whereas if the lower bound is negative, this accuracy is simply the upper bound $\mathbb{E}_r[S^{SC}_{A,r}]$.

C. Effects of quantum channels

Given that we can efficiently constrain the measurement-averaged entanglement, it is natural to ask whether we can say anything about how it changes under quantum

operations. Suppose that after preparing ρ_m (for simplicity, here we again omit subregion labels) we want to know how its entanglement entropy is modified by a known m-independent completely positive trace-preserving (CPTP) linear map,

$$\rho_m \to \mathcal{E}(\rho_m) \equiv \rho_{m,\mathcal{E}}. \tag{26}$$

We will denote the entanglement entropy of $\rho_{m,\mathcal{E}}$ by $S_{m,\mathcal{E}}$. An important property of the quantum relative entropy is that it is monotonically decreasing under CPTP maps [57], i.e., if $\rho_m \to \rho_{m,\mathcal{E}}$ and $\rho_m^C \to \rho_{m,\mathcal{E}}^C = \mathcal{E}(\rho_m^C)$, then

$$D_{m,\mathcal{E}} \equiv \mathrm{Tr}[\rho_{m,\mathcal{E}}(\log \rho_{m,\mathcal{E}} - \log \rho_{m,\mathcal{E}}^C)] \tag{27}$$

satisfies $D_{m,\mathcal{E}} \leq D_m$. This property implies that if the map $\mathcal{E}$ increases the measurement-averaged quantum-classical entanglement entropy, it must also increase the true measurement-averaged entanglement entropy:

$$\mathbb{E}_r[S_{r,\mathcal{E}}^{SC}] \geq \mathbb{E}_r[S_r^{SC}] \implies \mathbb{E}_m[S_{m,\mathcal{E}}] \geq \mathbb{E}_m[S_m], \tag{28}$$

where we have defined $S_{r,\mathcal{E}}^{SC} \equiv -\mathrm{Tr}[\mathcal{E}(\rho_r^S)\log \mathcal{E}(\rho_{m_r}^C)]$, i.e., the channel is applied to the shadow and also to the classical estimate for the postmeasurement density matrix $\rho_{m_r}^C$. The quantity $\mathbb{E}_r[S_{r,\mathcal{E}}^{SC}]$, like $\mathbb{E}_r[S_r^{SC}]$, can therefore be determined entirely through classical postprocessing of the experimentally determined shadows ρ_r^S.

VI. STATISTICAL FLUCTUATIONS

Above, we have shown that measurement-averaged entanglement properties can be bounded using particular quantum-classical cross-correlations. These bounds hold provided that the averages over runs of the experiment have converged, i.e., if $\mathbb{E}_r[S_r^{SC}] = \mathbb{E}_m[S_m^{QC}]$, but in practice the number of runs R is finite. Consequently, these bounds will only be accurate to within an error that decays as $\sim R^{-1/2}$.

In this section, we discuss the statistical fluctuations of S_r^{SC} over runs, focusing for simplicity on the case of a single qubit. This example will illustrate the role played by small eigenvalues of $\rho_{m_r}^C$ in the convergence of the average of S_r^{SC}. Some care is required in directly applying bounds on the variance in Ref. [34] since these diverge as ρ_m^C approaches a pure state.

The mean-squared fluctuation of S_r^{SC} around $S_{m_r}^{QC}$ for a particular outcome $m = m_r$ is

$$(\sigma_m^{SC})^2 = \sum_{z,U} P_{z,U|m}\mathrm{Tr}\left[\left(\rho^S(z,U) - \rho_m\right)\log \rho_m^C\right]^2, \tag{29}$$

with $\rho^S(z,U)$ given as usual by Eq. (8) [see above Eq. (7)], and $P_{z,U|m}$ is the probability that we have acted with U and observed z given outcomes m. To calculate σ_m^{SC}, we require certain properties of the first three moments of the Haar distribution over the unitary group. Haar invariance implies that

$$\sum_U p_U \prod_{k=0}^{n-1} U_{i_k 0} U_{j_k 0}^* = C_n \sum_\pi \prod_{k=0}^{n-1} \delta_{i_k j_{\pi(k)}}, \tag{30}$$

where $\sum_\pi$ denotes a sum over all permutations π of n elements. By contracting indices in Eq. (30), it is straightforward to show for $n \leq 3$ that the coefficients $C_n = [(n+1)!]^{-1}$. This expression holds for Haar-random unitary operations U as well as those drawn from the Clifford group, because the latter forms a 3-design [58,59].

Using Eq. (30) in Eq. (29), we find that $(\sigma_m^{SC})^2$ can be expressed, up to prefactors, as the sum of three contributions: (i) the variance v_m of $-\log \rho_m^C$ with respect to ρ_m, (ii) the variance $v_{\mathbb{1}}$ of $-\log \rho_m^C$ with respect to the maximally mixed state $\mathbb{1}/2$, and (iii) the difference $\Delta_{m\mathbb{1}}$ between the expectation values of $-\log \rho_m^C$ computed with respect to ρ_m and $\mathbb{1}/2$. In full,

$$(\sigma_m^{SC})^2 = \frac{3}{2}(v_m + v_{\mathbb{1}}) + \frac{1}{2}\Delta_{m\mathbb{1}}^2. \tag{31}$$

where

$$\begin{aligned} v_m &= \mathrm{Tr}[\rho_m(\log \rho_m^C)^2] - \mathrm{Tr}[\rho_m \log \rho_m^C]^2, \\ v_{\mathbb{1}} &= \mathrm{Tr}[(\mathbb{1}/2)(\log \rho_m^C)^2] - \mathrm{Tr}[(\mathbb{1}/2)\log \rho_m^C]^2, \\ \Delta_{m\mathbb{1}} &= \mathrm{Tr}[(\rho_m - \mathbb{1}/2)\log \rho_m^C]. \end{aligned} \tag{32}$$

These results make clear that no matter how accurate our simulation, as ρ_m^C approaches a pure state and hence has eigenvalues approaching zero, the variance $(\sigma_m^{SC})^2$ diverges.

Consider, then, the scenario in which the minimum eigenvalue of ρ_m^C is lower bounded by $\epsilon \ll 1$. It is straightforward to impose this condition in practice since we have the freedom to choose ρ_m^C. For example, given a classical simulation that outputs a prediction for ρ_m^C, we could modify the output by passing ρ_m^C through a weak depolarizing channel. It can then be verified from Eqs. (31) and (32) that $(\sigma_m^{SC})^2 = O(\log^2[1/\epsilon])$ for small ϵ. The total variance relevant to experiment is simply the sum of (i) $\mathbb{E}_r[(\sigma_{m_r}^{SC})^2]$ and (ii) the variance of $S_{m_r}^{QC}$ over m_r. For $\rho_{m_r}^C$ having a minimum eigenvalue no smaller than ϵ, it is clear that contribution (ii) is itself $O(\log^2[1/\epsilon])$.

In the case of a single qubit it can be verified that the total variance of S_r^{SC} over runs is upper bounded by $3\log^2[1/\epsilon] + O(\epsilon)$. The numerical prefactor is specific to the case of a single qubit but the $O(\log^2[1/\epsilon])$ scaling of the variance is quite general. Moreover, this upper bound on the error is independent of the quality of the simulation. Suppressing the fluctuations in the average of S_r^{SC} to

well below the mean therefore requires a number of runs R scaling as $R \sim \log^2[1/\epsilon]/(\mathbb{E}_r[S_r^{SC}])^2$.

This section concludes our general discussion of the bounds on the measurement-averaged entanglement entropy. In summary, the average postmeasurement entanglement entropy of a subregion A can be upper and lower bounded, respectively, by cross-correlations $\mathbb{E}_r[S_{A,r}^{SC}]$ and $\mathbb{E}_r[S_{A,r}^{SC}] - \mathbb{E}_r[S_{AB,r}^{SC}]$, where subregion B does not overlap with A. These cross-correlations take as input (i) experimentally determined shadows ρ_r^S extracted from a quantum simulation and (ii) classical estimates for postmeasurement density matrices $\rho_{m_r}^C$. Each bound converges as a standard Monte Carlo average having variance $\sim \log^2[1/\epsilon]$.

These results reveal that the accuracy with which we can know the entanglement entropy is set by the separation between the bounds, i.e., $\mathbb{E}_r[S_{AB,r}^{SC}]$. As the classical simulation is improved, $\mathbb{E}_r[S_{AB,r}^{SC}]$ decreases and eventually approaches $\mathbb{E}_m[S_{AB,m}]$ in the limit of a perfect simulation. Since the quality of the classical simulation controls the quality of our bound, it will be useful to investigate a measurement-induced collective phenomenon that is associated with the breakdown of classical simulations.

VII. ENTANGLEMENT TRANSITION

In this section we consider the application of our approach to study the measurement-induced entanglement transition in random quantum circuits [7,8]. Our focus is on one-dimensional chains of qubits evolved under Haar-random two-qubit unitary gates and single-qubit projective measurements [6]. Unitary gates are arranged in a brickwork pattern and measurements are performed at a fixed rate p per qubit (for an illustration, see Fig. 2). Previous work on this model has revealed a transition between volume-law entangled states for $p < p_c$ and area-law entangled states for $p > p_c$ [5–8], with the critical point estimated as $p_c \simeq 0.16$ [60]. To clarify the notation, p refers to the probability that we choose to measure a qubit, while P_m is the Born probability corresponding to a set of outcomes m.

This entanglement transition is a useful setting for testing our idea because it corresponds to the point at which classical simulations break down: for $p < p_c$ the classical memory required to describe the state is exponential in the number L of qubits, whereas for $p > p_c$ it is expected that the required memory is only linear in L. To emphasize the limitations of classical memory, we will construct cross-correlations between exact numerics (representing the experiment or quantum simulation) and approximate numerics based on MPSs restricted to finite bond dimension χ (the classical simulation). The classical memory required for the MPS simulation then scales only as $\sim L\chi^2$. We stress that, in this illustrative example, both kinds of simulation are carried out on a classical computer; the phrases "quantum simulation" and "classical simulation" are an allusion to how our idea could be implemented in experiment (see, e.g., the related calculation in Ref. [31]).

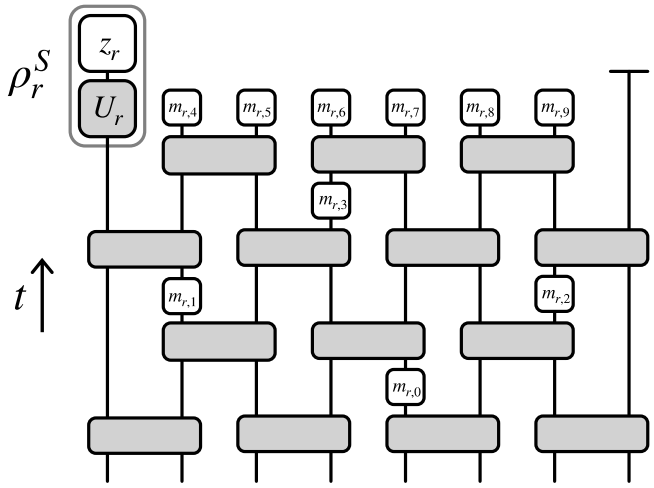

FIG. 2. Probe of measurement-induced entanglement transition. In each run r, L initially unentangled qubits are evolved through a circuit of depth t involving two-qubit Haar-random unitary operations (wide gray boxes) and, with a probability p at each time step, single-qubit measurements of Z (small white boxes, with outcomes $m_{r,0}, \ldots, m_{r,3}$ in the figure). At the final time, all bulk qubits are measured (here, outcomes $m_{r,4}, \ldots, m_{r,9}$). One then extracts a shadow ρ_r^S from the left boundary qubit by applying a single-qubit random unitary U_r and subsequently measuring Z (with result z_r). The outcomes $m_r = (m_{r,0}, \ldots, m_{r,9})$ are then used as input to a classical calculation, giving an estimate $\rho_{m_r}^C$ for the postmeasurement density matrix of the left qubit, and from ρ_r^S and $\rho_{m_r}^C$ we construct S_r^{SC}, which is averaged over r. For illustration, here we show $N = 8$ and $t = 4$, although for numerical calculations we fix $t = 4L$.

Care is required when sampling measurement outcomes: while the effects of particular measurement outcomes can be "forced" in a classical simulation (through the application of a desired projection operator), they cannot be forced in experiment. Therefore, here we must sample the outcomes of measurements according to the Born rule in the quantum simulation (i.e., with Born probabilities calculated using exact numerics) and then force these outcomes in the classical simulation.

We choose to work with chains having open rather than periodic boundary conditions, since MPS simulations are then much more efficient [61]. Because the measurement-induced entanglement transition appears to have a dynamic critical exponent of unity [5,6], we evolve the system for a time $t = 4L$, corresponding to $2L$ two-site unitary operations on each bond. After each such operation, we measure each of the two evolved qubits with a probability p, with outcomes sampled as described in the previous paragraph and with the caveat that during the evolution we choose not to measure the qubits at the left and right ends of the

chain. Following the measurement step, we truncate the bond dimension in the MPS simulation to χ. The bond dimension therefore increases from a maximum of χ to 4χ through the unitary operation, is potentially decreased by measurement, and finally is truncated back to a maximum of χ. At the final time, we have an exact representation of the quantum state (from the quantum simulation) and a MPS with bond dimension χ. In Sec. VIII, we discuss a way to characterize the postmeasurement state.

A. Upper bound

To probe quantum correlations, we must focus on density matrices of small numbers of qubits. This is because the variance of S_r^{SC} grows exponentially with the number of qubits being investigated [34]. The local probe that we choose is as follows: at $t = 4L$, we measure all but the left- and right-most qubits in the chain and we then try to estimate the entanglement entropy of the left qubit (this is equal to the entanglement entropy of the right qubit, since the overall state is pure); our protocol is represented in Fig. 2.

Our numerical (Monte Carlo) average over runs $\mathbb{E}_r[\cdots]$ will, in this section, also include an average over unitary gates used to construct the quantum circuit. Since the postmeasurement density matrices of the left qubit are determined not only by outcomes m_r observed in run r but also by the unitary gates in that run, here we will use the more general notation ρ_r rather than ρ_{m_r}. It is important to note that m_r represents the list of outcomes recorded during evolution and also at the final time. In this notation, the classical estimate for ρ_r in run r is ρ_r^C and the shadow is ρ_r^S, with, e.g., $S_r = -\mathrm{Tr}[\rho_r \log \rho_r]$ and $S_r^{SC} = -\mathrm{Tr}[\rho_r^S \log \rho_r^C]$. The upper bound in Eq. (20) is then written $\mathbb{E}_r[S_r] \leq \mathbb{E}_r[S_r^{QC}] = \mathbb{E}_r[S_r^{SC}]$. Since here we are using exact numerics in place of an actual quantum simulation, for numerical convenience we directly determine ρ_r and then average S_r^{QC} rather than S_r^{SC}. The result is the same for a large number of runs.

A reason for considering the postmeasurement entanglement between the boundary qubits in the present setting is that it is straightforward to understand some of the effects of a finite bond dimension. For any χ, Eq. (20) guarantees that $\mathbb{E}_r[S_r^{QC}] \geq \mathbb{E}_r[S_r]$, with the difference expected to increase with L. On the other hand, for finite χ we can compute ρ_r^C as a product of essentially random finite-dimensional matrices; without fine tuning, there is a gap between the two leading Lyapunov exponents characterizing this product. As a consequence, $\mathbb{E}_r[S_r^{CC}]$ must decay exponentially with L for any finite χ. Since $\mathbb{E}_r[S_r]$ is L independent for $p < p_c$ and decays as a power of L for $p = p_c$, we see that at fixed χ and for sufficiently large L, the classical estimate for the measurement-averaged entanglement $\mathbb{E}_r[S_r^{CC}]$ should lower bound the true entanglement entropy $\mathbb{E}_r[S_r]$. Having an approximate lower bound of this kind is useful because, by increasing χ, we can expect the chain of inequalities $\mathbb{E}_r[S_r^{CC}] \lesssim \mathbb{E}_r[S_r] \leq \mathbb{E}_r[S_r^{QC}]$ to become more restrictive. We defer a discussion of the rigorous lower bound in Eq. (25) to Sec. VII C.

First we sweep across the transition. In Fig. 3(a), we show $\mathbb{E}_r[S_r]$, $\mathbb{E}_r[S_r^{QC}]$ and $\mathbb{E}_r[S_r^{CC}]$ for $L = 20$ and various χ. On increasing χ, the window between $\mathbb{E}_r[S_r^{CC}]$ and $\mathbb{E}_r[S_r^{QC}]$ becomes narrower and, as discussed above, $\mathbb{E}_r[S_r]$ should lie within this window at large L. Interestingly, $\mathbb{E}_r[S_r^{QC}]$ departs from the true measurement-averaged entanglement entropy at a much larger value of p than $\mathbb{E}_r[S_r^{CC}]$. The splitting of $\mathbb{E}_r[S_r^{QC}]$ and $\mathbb{E}_r[S_r^{CC}]$ signifies the breakdown of the simulation: the apparent agreement between $\mathbb{E}_r[S_r^{CC}]$ and $\mathbb{E}_r[S_r]$ even for small p is an artifact of the ensemble average. This is to say that although $\mathbb{E}_r[S_r^{CC}]$ and $\mathbb{E}_r[S_r]$ appear to agree, we know that S_r^{CC} and S_r disagree for individual runs r, because $\mathbb{E}_r[S_r^{QC}]$ and $\mathbb{E}_r[S_r]$ disagree.

Turning now to the critical regime $p = 0.16$, in Fig. 3(b) we investigate the effect of increasing L for various χ. As expected, the decay of $\mathbb{E}_r[S_r]$ is consistent with a power law $\sim L^{-\alpha}$ and we find numerically that $\alpha \approx 0.6$. For each χ we see that, as L is increased, there is a point beyond which $\mathbb{E}_r[S_r^{QC}]$ deviates from this power-law decay and instead begins to increase.

It is natural to ask how the system size L at which this occurs depends on χ. This dependence will control the classical memory required to study the transition in experiment. In Fig. 3(c), we show that $\mathbb{E}_r[S_r^{QC}]$ can be collapsed according to the scaling form

$$\mathbb{E}_r[S_r^{QC}] \simeq A L^{-\alpha} f\left(\chi L^{-\lambda}\right), \tag{33}$$

where A is the prefactor of the $L^{-\alpha}$ decay in $\mathbb{E}_r[S_r]$ and $f(x)$ is a function satisfying $f(x \to 1) = 1$ for large x (and which is large at small x). In Fig. 3(c), we have set the exponent $\lambda = 2$ but we discuss this further below. This collapse is an experimentally observable signature of measurement-induced criticality, which can be obtained without postselection through the average $\mathbb{E}_r[S_r^{SC}]$. We discuss this signature, and the resources required to observe it, in Sec. VII B.

Note that here we have not used our method to determine the critical point. Instead, we have relied on an existing high-accuracy numerical estimate for the critical point p_c from Ref. [60] and in Figs. 3(b) and 3(c) we have studied cross-correlations at this point. More generally, the critical point of a measurement-entanglement transition is not known *a priori* and, as we now discuss, a variation of the above analysis can be used to locate p_c in large-scale experiments. Under the assumption that the volume-law entangled states generated at $p < p_c$ cannot be represented using polynomial classical memory, the entanglement transition is a "simulability transition". As an order parameter,

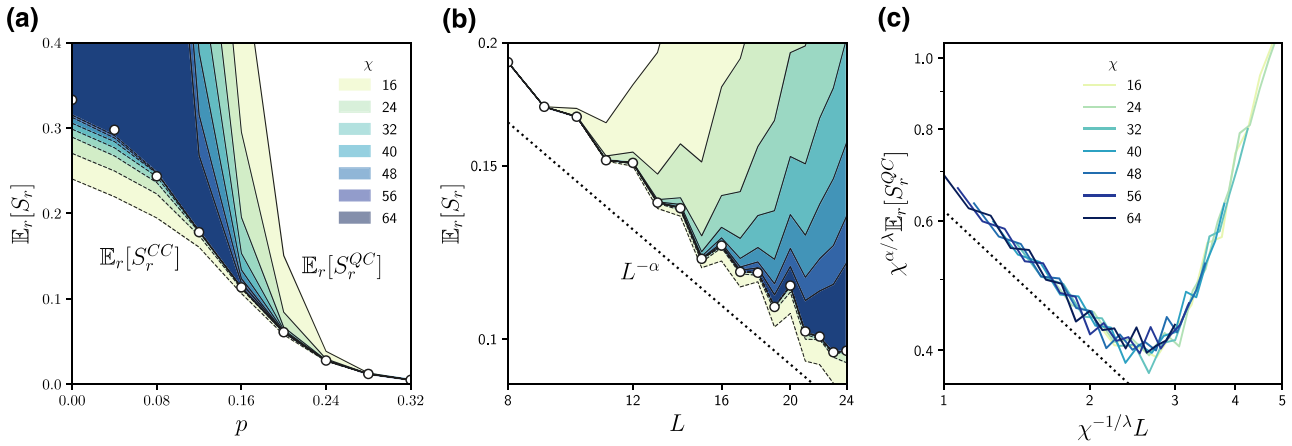

FIG. 3. Estimates for average entanglement entropy of an edge site after measuring bulk qubits. (a) $L = 20$ with various p and χ. The different shaded regions, corresponding to different χ, have lower edges $\mathbb{E}_r[S_r^{CC}]$ (indicated by dashed gray lines) and upper edges $\mathbb{E}_r[S_m^{QC}]$ (indicated by solid gray lines). Narrower shaded regions correspond to larger χ (see the legend). The open circles correspond to the exact average entropy $\mathbb{E}_r[S_r]$. (b) Entanglement in the critical regime, $p = 0.16$, and for various system sizes L. The dotted black line shows a power-law fit $\sim L^{-\alpha}$ to $\mathbb{E}_r[S_r]$ (open circles). The exponent $\alpha = 0.62 \pm 0.02$ and the fit is offset from the data for clarity. (c) Scaling collapse of $\mathbb{E}_r[S_r^{QC}]$, corresponding to the upper edges of the shaded regions in (b), for various χ. For this collapse we use $\lambda = 2$, and we discuss this exponent in detail in Sec. VII B. The dotted line shows a decay of $\sim L^{-\alpha}$, as in (b).

one can therefore use the observable $\mathbb{E}_r[S_r^{SC} - S_r^{CC}]$. As we have shown in Fig. 3(a), a failure to simulate the system is manifest in a nonzero order parameter. The volume-law phase $p < p_c$ can therefore be identified as the regime in which the classical memory $\sim L\chi^2$ required to decrease the order parameter grows exponentially with L. On the other hand, in the area-law phase $p > p_c$, the order parameter can be suppressed using polynomial classical memory. Another candidate order parameter, which would also be viable in this setting, is $\mathbb{E}_r[S_{AB,r}^{SC}]$, where A and B are the boundary qubits, and we discuss this further in Sec. VII C.

B. Resource requirements

The classical memory required to store a MPS scales as $\sim L\chi^2$. For $p < p_c$, we expect that the bond dimension required to obtain a reasonable approximation to the true quantum state is exponential in L, so determining the measurement-averaged entanglement there is presumably a lost cause. At the critical point $p = p_c$ itself, it is suggested in Fig. 3(c) that with bond dimension $\chi \gtrsim L^\lambda$ we can find a restrictive bound on $\mathbb{E}_r[S_r]$. This is plausible because, prior to measuring all but the left and right qubits, the half-chain entanglement entropy at $p = p_c$ is proportional to $\log L$ [7,8]. Since the half-chain entanglement is upper bounded by $\log \chi$, one would only need a bond dimension polynomial in L to capture this.

To explore the χ dependence of $\mathbb{E}_r[S_r^{QC}]$ in detail, in Fig. 4(a) we calculate $\mathbb{E}_r[S_r^{QC}]/\mathbb{E}_r[S_r]$. There, we find that the convergence of $\mathbb{E}_r[S_r^{QC}]$ is exponential,

$$\mathbb{E}_r[S_r^{QC}]/\mathbb{E}_r[S_m] - 1 \propto e^{-\chi/\chi^{QC}(L)}, \tag{34}$$

with a constant of proportionality that is of order unity and approximately L independent. It can be verified that this is consistent with Fig. 4(b) provided that χ is not too much smaller than $\chi^{QC}(L)$. The behavior in Fig. 4(a) provides further evidence that there is a characteristic bond dimension $\chi^{QC}(L)$ beyond which S_r^{QC} and S_r are in good agreement and that this bond dimension increases with L. Following Eq. (33), we expect $\chi^{QC}(L) \sim L^\lambda$ and in Fig. 4(b) we show $\chi^{QC}(L)$ as a function of L. Our results are consistent with a power-law growth having $\lambda \lesssim 2$; a more accurate determination of λ will require access to larger system sizes. Combining Eqs. (33) and (34), we see that the function $f(x)$ takes the form

$$f(x) = 1 + Be^{-x/x_0}, \tag{35}$$

where B and x_0 are constants. For the particular model that we consider, we find from Fig. 4 that $B \approx 15$ while $x_0 \approx 0.04$. The observation that $\lambda \lesssim 2$ implies that a good MPS representation of the quantum state need only occupy polynomial classical memory $L\chi^2 \sim L^{1+2\lambda} \lesssim L^5$.

The power-law scaling of the bond-dimension with a length scale echoes the theory of finite-entanglement scaling at conventional quantum critical points [62–64]. This theory predicts that a finite bond dimension χ introduces a finite correlation length $\xi \sim \chi^\kappa$ with an exponent κ that is a function of the central charge of the conformal field theory describing the critical point. That theory addresses the question of how much classical memory is required to study quantum criticality on a classical computer and it would be interesting to develop an analogous

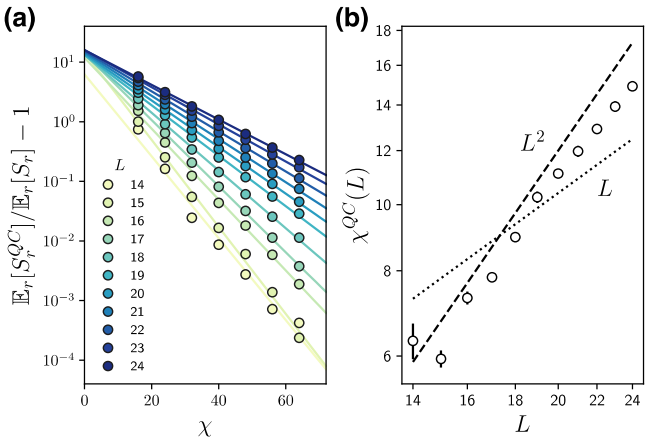

FIG. 4. Effect of varying the bond dimension χ at $p = 0.16$. (a) Decay of $\mathbb{E}_r[S_r^{QC}]/\mathbb{E}_r[S_r] - 1$ with χ for various L (open circles) and fits to exponential decays (solid lines). The decay rates give the parameter $\chi^{QC}(L)$ in Eq. (34). (b) Growth of $\chi^{QC}(L)$ with L (open circles), with logarithmic scaling of both axes, compared with power laws L (dotted) and L^2 (dashed).

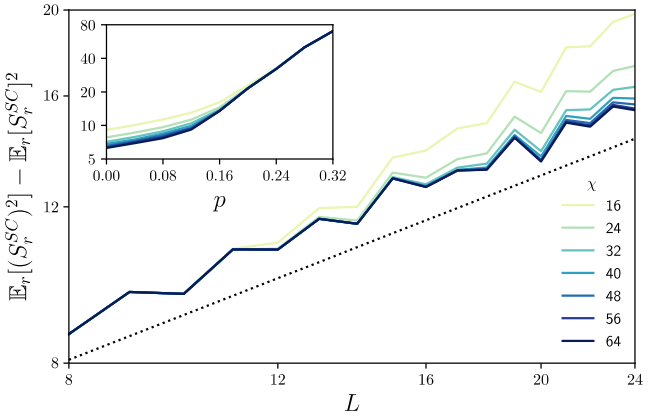

FIG. 5. Variance of S_r^{SC} over runs. The main panel shows (with a log-log scale) the variance as a function of L for $p = 0.16$ and various χ (see the legend). The dotted line shows a fit $\sim L^\beta$ to data for $\chi = 64$, with $\beta = 0.52 \pm 0.02$, and this is offset from the data for clarity. The inset shows the variance as a function of p for $L = 20$ and for the same values of χ as in the main panel (here, with a log-linear scale).

theory for measurement-induced criticality. In our notation, this would correspond to a theory for the convergence of $\mathbb{E}_r[S_r^{CC}]$ to $\mathbb{E}_r[S_r]$.

Our results above, on the convergence of $\mathbb{E}_r[S_r^{QC}]$ to $\mathbb{E}_r[S_r]$, address the quite different question of how much classical memory is required to observe measurement-induced criticality in a quantum simulator. The interpretation of the measurement-induced entanglement transition as a kind of replica-symmetry-breaking transition [65,66] suggests that the classical memory requirements are different in the two cases: writing S_r^{QC} as the $n \to 1$ limit of the object $[1-n]^{-1} \log \mathrm{Tr}[\rho_r (\rho_r^C)^{n-1}]$, it is clear that since $\rho_r \neq \rho_r^C$, the symmetry under exchange of replicas is reduced relative to $[1-n]^{-1} \log \mathrm{Tr}[(\rho_r^C)^n]$, which reproduces S_r^{CC} as $n \to 1$. In other words, the constraint of finite χ is a replica-symmetric perturbation in S_r^{CC} but not in S_r^{QC}.

Having discussed the classical memory requirements, we now turn to the time requirements. This is a question of how many experimental runs are required in order to wash out statistical fluctuations in S_r^{SC}. The variance of S_r^{SC} over runs is the sum of two contributions: the average of the variance over shadows ρ_r^S for each ρ_r and ρ_r^C, which is represented in Eq. (31), and the variance of S_r^{QC} over runs. Numerically, we find that the first of these two contributions dominates, although here we simply calculate the overall variance.

In the main panel of Fig. 5, we study the growth of the variance with L at $p = 0.16$ (in the critical regime). The data suggest that the growth is no faster than $\sim L^\beta$ for an exponent $\beta > 0$ and a fit to the $\chi = 64$ data indicates that $\beta \approx 0.5$ (see the caption of Fig. 5). As in Fig. 3(b), as L is increased at fixed χ, there is a point at which the simulation appears to break down. In Fig. 5, this breakdown manifests as an increase in the variance with decreasing χ. Before this point, where $\chi \gg \chi^{QC}(L)$, our results in Figs. 3(b) and 5 suggest that the number of experimental runs required to suppress the error to below the scale of the mean $\mathbb{E}_r[S_r] \sim L^{-\alpha}$ grows only as $L^{\beta+2\alpha} < L^2$.

This result shows that the transition in the behavior of the measurement-averaged von Neumann entanglement entropy can be observed using a number of runs that is polynomial in the system size. However, it is important to note that if one instead aims to bound the measurement-averaged purity, the statistical fluctuations are substantially smaller. This is because, as discussed below Eq. (12), the variance of the object that lower bounds $\mathbb{E}_r[\rho_r^2]$ is finite.

C. Lower bound

For simplicity, our focus has been on the upper bound on $\mathbb{E}_r[S_r]$ in Eq. (20) and we have not studied the lower bound in Eq. (25) numerically. As we have discussed in Sec. VI, in order to use Eq. (25), it would be necessary to consider a situation in which the overall state of the left and right boundary qubits is not quite pure. If their state is pure, the statistical fluctuations diverge. Here, we are concerned with both boundary qubits (A and B), so we will indicate subsystems explicitly.

A simple way to avoid the divergence of statistical fluctuations is to apply weak depolarizing channels to $\rho_{AB,r}^S$ and $\rho_{AB,r}^C$ in postprocessing, as described in connection with Eq. (28) and also in Sec. VI. If we apply these artificial

depolarizing channels to $\rho^S_{AB,r}$ and $\rho^C_{AB,r}$, we have

$$\begin{aligned}\rho^S_{AB,r} &\to \mathcal{E}(\rho^S_{AB,r}) = (1-4\epsilon)\rho^S_{AB,r} + \epsilon\mathbb{1},\\ \rho^C_{AB,r} &\to \mathcal{E}(\rho^C_{AB,r}) = (1-4\epsilon)\rho^C_{AB,r} + \epsilon\mathbb{1},\end{aligned} \tag{36}$$

and for $0 < \epsilon < 1/4$, all of the eigenvalues of $\mathcal{E}(\rho^C_{AB,r})$ are lower bounded by ϵ. The quantity $S^{SC}_{r,AB,\mathcal{E}} = -\mathrm{Tr}\,[\mathcal{E}(\rho^S_{AB,r})\log\mathcal{E}(\rho^C_{AB,m_r})]$ then has $|S^{SC}_{r,AB,\mathcal{E}}| = O(\log[1/\epsilon])$ for small ϵ. We denote by $\mathbb{E}_r[S_{r,AB,\mathcal{E}}]$ the average entanglement entropy of the set of density matrices $\mathcal{E}(\rho_{AB,m_r})$.

As discussed below Eq. (25), the average postmeasurement entanglement can be determined (rather than just upper bounded) to within a threshold $\mathbb{E}_r[S^{SC}_{r,AB,\mathcal{E}}] \geq \mathbb{E}_r[S_{r,AB,\mathcal{E}}]$. Regardless of the quality of the simulation, since $\mathbb{E}_r[S_{r,AB,\mathcal{E}}]$ itself has a lower bound of order $\epsilon\log(1/\epsilon)$ for small ϵ, it is clear that the accuracy with which we can determine the entanglement is no better than $O(\epsilon\log[1/\epsilon])$. Since the standard deviation of $\mathbb{E}_r[S^{SC}_{r,AB,\mathcal{E}}]$ is $O(\log[1/\epsilon])$, we see that the number of experimental runs required to suppress the fluctuations to below the scale of the mean $\mathbb{E}_m[S^{QC}_{m,AB,\mathcal{E}}]$ diverges as ϵ^{-2} on decreasing ϵ. This discussion nevertheless reveals a trade-off between the accuracy with which we determine the entanglement and the number of samples required.

In the context of the measurement-induced entanglement transition, at large L the entanglement entropy between the boundary qubits should decay as $\mathbb{E}_m[S_{A,m}] \sim L^{-\alpha}$. For an overall pure state, this implies that the minimum eigenvalue of $\rho_{A,m}$ itself decays as $\sim L^{-\alpha}$. On applying depolarizing channels in postprocessing, we destroy any correlations associated with eigenvalues on the scale of ϵ and hence we should set $\epsilon = O(L^{-\alpha})$. The number of experimental runs required to suppress fluctuations in $\mathbb{E}_r[S^{SC}_{r,A,\mathcal{E}}]$ and $\mathbb{E}_r[S^{SC}_{r,AB,\mathcal{E}}]$ to below $\sim L^{-\alpha}$ therefore grows only as $L^{2\alpha}\log^2[1/\epsilon] \sim L^{2\alpha}\log^2 L$ when using an artificial channel.

Through this section, we have studied the quantum-classical entanglement entropy in the context of measurement-induced criticality. We have shown that the manner in which classical simulations break down is an observable signature of criticality and we have provided evidence that, at the critical point, the classical resources required to observe scale-invariant features of measured quantum states are only polynomial in L.

VIII. DECODING PROTOCOL

It is important to understand the relation between $\mathbb{E}_r[S^{SC}_r]$ and the probe of Ref. [25]. For the sake of simplicity, in this section and in Sec. IX, we can consider a protocol in which the only randomness is in the measurement outcomes and so we return to the notational convention preceding Sec. VII. In Ref. [25], the authors consider a scenario in which the effects of many measurements, having outcomes m, are encoded in the state ρ_m of a reference qubit. A generalization of their decoding scheme to the situation in which one has an approximate classical simulation of the model is as follows: given an observed set of measurement outcomes m_r in run r, one (i) estimates the postmeasurement density matrix $\rho^C_{m_r}$, (ii) constructs a unitary decoder $V^C_{m_r}$ such that the Bloch vector of $V^C_{m_r}\rho^C_{m_r}[V^C_{m_r}]^{-1}$ is parallel to the $+Z$ axis, (iii) applies the decoder to the true postmeasurement density matrix ρ_{m_r}, (iv) measures Z, and (v) averages the results z_r over runs of the experiment. If ρ_{m_r} is pure and the calculation on a classical computer yielding $\rho^C_{m_r}$ is perfect, the result of the measurement in step (iv) is $z_r = 1$ with certainty. If ρ_m is maximally mixed, the result is $z_r = \pm 1$ with equal probability.

This approach naturally gives a bound on a measurement-averaged property of the density matrix, as we now discuss, although this bound is distinct from the one in our Eq. (20). It will be convenient to define γ_m and γ^{CC}_m by $\mathrm{Tr}[\rho_m^2] = \frac{1}{2}[1+(\gamma_m)^2]$ and $\mathrm{Tr}[(\rho^C_m)^2] = \frac{1}{2}[1+(\gamma^{CC}_m)^2]$, respectively, where $0 \leq \gamma_m, \gamma^{CC}_m \leq 1$. Note that we then have $V^C_m\rho^C_m[V^C_m]^{-1} = \frac{1}{2}(1+\gamma^{CC}_m Z)$, where $\frac{1}{2}(1+\gamma^{CC}_m)$ is the classical estimate for the probability that the Z measurement returns $z_r = 1$. If we apply the decoder V^C_m to ρ_m and then measure Z, the probability of finding $z_r = 1$ is, instead,

$$\frac{1}{2}(1+\gamma^{QC}_m) \equiv \langle 1|V^C_m\rho_m[V^C_m]^{-1}|1\rangle\,, \tag{37}$$

which defines the quantum-classical object γ^{QC}_m satisfying $\gamma^{QC}_m \leq \gamma_m$. Here, equality is achieved when the Bloch vectors of ρ^C_m and ρ_m are parallel (but not necessarily equal). This is because an imperfect decoder will generate a density matrix $V^C_m\rho^C_m[V^C_m]^{-1}$, the Bloch vector of which is canted relative to the $+Z$ axis, and hence a measurement of Z has a lower probability of yielding the result $z_r = 1$. If we repeat the experiment many times, averaging z_r over runs, the result is

$$\mathbb{E}_r[z_r] = \mathbb{E}_m[\gamma^{QC}_m] \leq \mathbb{E}_m[\gamma_m]. \tag{38}$$

Although Eq. (20) does bound a measurement-averaged property of the ensemble of ρ_m, it does not provide us with information on a standard entanglement measure.

On a practical level, the scheme presented earlier in this work is based on classical postprocessing rather than the application of a conditional decoding unitary V^C_m. The former approach is simpler in experimental settings, where decoherence time scales may be too short for one to determine and then apply a measurement-conditioned unitary. That said, as we now show, the quantity $\mathbb{E}_m[\gamma^{QC}_m]$ that is determined via the scheme in Ref. [25] can also be

determined simply by classical postprocessing and so we expect that if either one is experimentally viable, then both should be.

To see how to determine $\mathbb{E}_m[\gamma_m^{QC}]$ through classical postprocessing, we need only consider the average of Eq. (37) over outcomes. In run r, corresponding to outcome m_r, we extract a shadow ρ_r^S and calculate a matrix-valued weight

$$W_{m_r} = 2[V_{m_r}^C]^{-1} |1\rangle \langle 1| V_{m_r}^C - \mathbb{1}. \tag{39}$$

For this W_{m_r}, we have

$$\mathbb{E}_r[\rho_r^S W_{m_r}] = \mathbb{E}_m[\gamma_m^{QC}]. \tag{40}$$

A different quantum-classical cross-correlation, sharing some features with Eq. (40) but based on scalar- rather than matrix-valued cross-correlations, has recently been implemented in a quantum simulator [31]. In the above notation, that approach corresponds to replacing W_{m_r} with $\text{sign}(\text{Tr}[\rho_{m_r}^C Z])Z$.

Inverting this discussion, we can also ask what would be the analogue of our scheme for determining $\mathbb{E}_r[S_r^{QC}]$ if we were to use measurement-conditioned unitary decoders rather than classical postprocessing. A hint comes from the fact that we can interpret S_m^{QC} as the expectation value of the m-dependent observable $-\log \rho_m^C$ with respect to the true density matrix ρ_m. In fact, the protocol would be almost identical to that in Ref. [25], with only a minor difference in the step (v) indicated at the start of this section. That is, having extracted the measurement outcomes m_r in each run r, used them as inputs to calculations giving $\rho_{m_r}^C$ and $V_{m_r}^C$, applied $V_{m_r}^C$ to ρ_{m_r}, and measured Z (all before the qubits decohere), the only difference is in the number that we should average. If instead of averaging eigenvalues $z_r = \pm 1$ of Z, which gives $\mathbb{E}_r[z_r] = \mathbb{E}_m[\gamma_m^{QC}]$ in the limit of a large number of runs, one instead averages the corresponding eigenvalues $-\log[(1 + z_r \gamma_{m_r}^{CC})/2]$ of the negative logarithm of the density matrix $\rho_{m_r}^C$, the result converges to $\mathbb{E}_r[S_r^{QC}]$.

While the measurement-averaged results from a decoding scheme giving $\mathbb{E}_m[S_m^{QC}]$ are the same as from classical postprocessing using shadows, the statistical fluctuations are likely to be much smaller. This is because if ρ_m^C is a good estimate for ρ_m, in the decoding scheme one is less likely to be affected by small eigenvalues of ρ_m^C. This decrease in the scale of statistical fluctuations comes at the cost of having to apply a measurement-conditioned unitary operation. A further issue with a decoding scheme is that it is unclear how to generalize it to study postmeasurement density matrices of multiple qubits without introducing multiqubit unitary operations. Within a shadows scheme involving only classical postprocessing, the extension is immediate: one can construct multiqubit shadows simply as tensor products of single-qubit shadows.

IX. ENTANGLEMENT NEGATIVITY

Our focus in this work has been on bounding the measurement-averaged von Neumann entanglement entropy. While the bounds in Eq. (25) also hold in the presence of noise, i.e., when we have access only to a mixed state, the von Neumann entanglement is then no longer a sensitive probe of quantum correlations. In particular, it can be nonzero even when the overall density matrix is diagonal.

This concern motivates the question of whether it is possible to bound measures of mixed-state entanglement. A prominent probe is the entanglement negativity [67], which can be defined for the density matrix ρ_{AB} of a bipartite system AB as

$$\mathcal{N}(\rho_{AB}) = -\text{Tr}[P^{(-)}(\rho_{AB}^{T_A})\rho_{AB}^{T_A}]. \tag{41}$$

Here, $\rho_{AB}^{T_A}$ denotes the partial transpose of the density matrix for subsystem A and $P^{(-)}(\rho_{AB}^{T_A})$ is the projector onto the space spanned by the eigenvectors of $\rho_{AB}^{T_A}$ with negative eigenvalues. The negativity has the appealing property of vanishing for unentangled states and not increasing under local operations and classical communication. Now observe that we can bound the average of the postmeasurement negativity $\mathcal{N}(\rho_{AB,m}) = -\text{Tr}[P^{(-)}(\rho_{AB,m}^{T_A})\rho_{AB,m}^{T_A}]$ using

$$\mathbb{E}_m[\mathcal{N}(\rho_{AB,m})] \geq -\mathbb{E}_r[P^{(-)}(\rho_{AB,m_r}^{C,T_A})\rho_{AB,r}^{S,T_A}]. \tag{42}$$

Here, ρ_{AB,m_r}^{C,T_A} is the partial transpose of the classical estimate for the density matrix of AB given outcomes m_r, which is used to construct the projector $P^{(-)}(\rho_{AB,m_r}^{C,T_A})$, and $\rho_{AB,r}^{S,T_A}$ is the partial transpose of the shadow in run r. Equation (42) shows that we can lower bound the measurement-averaged entanglement negativity by maximizing the right-hand side over projection operators.

X. DISCUSSION AND OUTLOOK

The randomness of the quantum measurement process prevents us from directly observing the effects of many measurements in experiment without an exponential postselection overhead. Cross-correlations (and cross entropies) between quantum experiments and classical simulations [14,18,29–31,33,68] provide a way to avoid this overhead but in general do not provide information on intrinsic properties of quantum states. For this reason, there appeared to be a division between experiments studying the effects of measurement and more conventional experiments that study the response to deterministic perturbations. Because the latter can be efficiently reproduced, effects of the perturbation on intrinsic properties of the system can be determined by averaging over experiments. In this work, we have resolved this division by

showing that certain cross-correlations provide unambiguous bounds on intrinsic properties of measured quantum states.

Our first step was to extend the randomized measurement framework [69] to the characterization of quantum states that are not efficiently reproducible. To do this, we synthesized shadows [34] with the cross-correlation approach of Refs. [14,18,29,31]. We then identified cross-correlations between experimentally determined shadows and the results of classical simulations that act as both upper and lower bounds on the postmeasurement von Neumann entanglement entropy. Related cross-correlations were shown to lower bound the purity and negativity.

Note that the randomized measurement protocol requires only that individual qubits can be measured in any of the Pauli-X, -Y, or -Z bases. In the postmeasurement setting, in each run r of the experiment, one extracts a set of measurement outcomes m_r in addition to a shadow ρ_r^S of a finite number of qubits. Our bounds can then be determined in postprocessing from a classical computation taking ρ_r^S and m_r as input.

The upper bound in Eq. (20) can be applied quite generally and the only restriction is that the subregion of interest should consist of a small finite number of qubits. This is because statistical fluctuations of $S_{A,r}^{SC}$ grow rapidly with the support of A (as for standard probes of the entanglement entropy). The lower bound in Eq. (25), on the other hand, is only restrictive when we can identify another subregion B such that AB is almost pure. The quantum-classical object $\mathbb{E}_r[S_{AB,r}^{SC}] \geq \mathbb{E}_m[S_{AB,m}]$ can then be made small and hence the bounds in Eq. (25) can be made restrictive. This constraint provides strong motivation for experimental protocols of the kind discussed in, e.g., Refs. [43,44] and our Sec. VII, where the effects of a large number of measurements are ultimately encoded in the entanglement between just two qubits.

Interestingly, our bounds suggest that we can view the postselection problem as a variational problem, where $\mathbb{E}_r[S_r^{SC}]$ is an objective function taking experimental data as input. For example, if the classical simulation has a parameter (or parameters) μ, then by minimizing $\mathbb{E}_r[S_r^{SC}]$, one can optimize the bound on $\mathbb{E}_m[S_m]$, thereby improving the model from experimental data. A concrete application is to quantum error-correction schemes [1]; in that setting, one is interested in the effects that large numbers of syndrome measurements have on the states of logical degrees of freedom.

There is, however, a possible pitfall in constructing a variational scheme: the above parameters μ must be chosen independently of the random unitary operations U_r and random measurement results z_r used to construct the shadows. Otherwise, the average of S_r^{SC} over runs is not guaranteed to converge to the average of S_m^{QC} over outcomes. A straightforward way to implement a valid variational scheme is to choose μ based on one set of experimental runs and then to compute the average of S_r^{SC} using this μ and a distinct set of runs. In the context of machine learning (for a different application of machine-learning techniques in the present context, see Ref. [27]), this simply corresponds to a division into training and test data.

When applying the ideas in this work to data obtained in current quantum simulators, it is important to account for the presence of noise. Significant statistical errors arise when ρ_m^C has small eigenvalues (see, e.g., the behavior at large p in the inset of Fig. 5). Very recently, in Ref. [70] it has been shown that the idea of common random numbers can be generalized to shadow estimation; this procedure reduces statistical errors provided that one has access to a classical estimate for the shadow, which can itself be estimated from a classical estimate for the density matrix. In our case, the scheme corresponds to averaging the difference between S_r^{SC} and $-\mathrm{Tr}[\rho_r^{SC} \log \rho_{m_r}^C]$ over runs of the experiment, where ρ_r^{SC} is a "shadow" that is constructed from a classically simulated experiment in which one applies U_r to $\rho_{m_r}^C$ and measures in the computational basis (to be contrasted with ρ_r^S, which is constructed from U_r and ρ_{m_r}). The basic principle is that while the above difference certainly converges to $\mathbb{E}_m[S_m^{QC}] - \mathbb{E}_m[S_m^{CC}]$, the errors in the two contributions are correlated and partially cancel one another.

It is important to note that in current quantum simulation platforms, it is often simpler to make all measurements simultaneously and destructively [2–4]. We must then ask which measurement-induced collective phenomena are observable given this constraint. Remarkably, even in such an experiment, our scheme allows one to probe the effect that measuring one subsystem has on the entanglement entropy of another subsystem, as in Refs. [43,44]. Moreover, given existing data from experiments involving randomized measurements [71–73], through purely classical postprocessing we can already study ensembles of postmeasurement states.

To see how this works, consider a tripartite system with subsystems denoted A, B, and B', prepared in an entangled state, and suppose that we are interested in how measurements of B, but not B', affect the entanglement entropy of A. In each run prior to measuring all degrees of freedom, it is necessary to act on A with random unitary operations U_r that will be used for shadows $\rho_{A,r}^S$. After measuring, the set of outcomes m_r in B should be used to construct a classical estimate ρ_{A,m_r}^C for the density matrix of A that is conditioned on outcomes in B but not in B', i.e., we simply do not use the information from the measurements in B'. By cross-correlating the shadow $\rho_{A,r}^S$ of A, which is obtained from the random unitary operations and measurement outcomes there, with $-\log \rho_{A,m_r}^C$, we arrive at the measurement-averaged entanglement entropy of A as if B' had not been measured. This scheme works because if we

do not use the outcomes of measurements in B', then by averaging over runs of the experiment we convert these measurements into local dephasing events and the effects of local quantum channels are strictly local.

Our approach should be contrasted with probes of statistical properties of measurement records, most notably the cross-entropy benchmark studied in the context of random circuit sampling [32]. The linear cross-entropy benchmark has also been advocated a resolution of the postselection problem for the measurement-induced entanglement transition in stabilizer circuits in Ref. [33]. The difference is that the linear cross-entropy benchmark is a cross-correlation between full probability distributions over measurement outcomes m, i.e., it is a cross-correlation of P_m and P_m^C, where P_m^C is the classical estimate for the probability of finding the set of outcomes m, whereas the cross-correlations discussed in this work are between few-body quantities conditioned on measurement outcomes, e.g., ρ_m and ρ_m^C. Focusing on few-body quantities has the advantage that in generic (nonstabilizer) systems, their fluctuations are much smaller. For example, if P_m^C is a product of probabilities for M different measurement outcomes, there are situations in which the number of experimental runs required to converge the average of P_m^C grows exponentially with M.

As an example of one of our quantum-classical cross-correlations, we have identified an observable signature of generic measurement-induced criticality. In particular, we have shown that for a cross-correlation at the critical point, the constraint of finite classical memory (parametrized by a finite bond dimension χ) introduces a length scale proportional to $\chi^{1/\lambda}$ with $\lambda \lesssim 2$. The classical memory required for our scheme therefore increases only as $L^{1+2\lambda}$. This behavior could have been anticipated from the fact that the exact measurement-averaged half-chain entanglement entropy (calculated before one measures all bulk qubits) grows logarithmically with L, while the theoretical maximum half-chain entanglement of an MPS grows logarithmically with χ.

This result hints toward a theory of finite-entanglement scaling at measurement-induced criticality, following Refs. [62–64]. A theory closer in spirit to those works would describe how simulations, corresponding to "classical-classical" probes in our terminology, behave as χ is increased. This would answer the question of how much classical memory is required to study measurement-induced criticality on a classical computer. The behavior of $\mathbb{E}_m[S_m^{QC}]$ that we have addressed instead describes the classical memory required to observe critical behavior in experiment.

Our work highlights the measurement-induced entanglement transition as the threshold beyond which we cannot observe the effects of our measurements. This threshold is mirrored in the quantum advantage in random circuit sampling [74] and emphasizes the fact that although quantum simulators have an immense capacity to store information, the randomness in its extraction is a deep limitation [75,76]. It is pertinent to ask whether, by cross-correlating quantum and classical simulations, we can learn more than from classical simulation alone.

ACKNOWLEDGMENTS

We are grateful to Sajant Anand, Yimu Bao, Matthew Fisher, Eun-Ah Kim, Katarzyna Macieszczak, Max McGinley, and Yaodong Li for useful discussions, to Zack Weinstein for helpful comments as well as for collaboration on related work [18], and to Matteo Ippoliti for pointing out the bound on the entanglement negativity discussed in Sec. IX. This research was supported by the Gordon and Betty Moore Foundation (S.J.G.), the U.S. Department of Energy, Office of Science, Office of High Energy Physics, under QuantISED Award No. DE-SC0019380 (S.J.G.), the National Science Foundation Quantum Leap Challenges Institute through Grant No. OMA-2016246 (E.A.), and a Simons Investigator Award (E.A.). Numerical calculations were carried out using the Lawrencium computational cluster resource provided by the IT Division at the Lawrence Berkeley National Laboratory (Supported by the Director, Office of Science, Office of Basic Energy Sciences, of the U.S. Department of Energy under Contract No. DE-AC02-05CH11231). Publication was made possible in part by support from the Berkeley Research Impact Initiative (BRII) sponsored by the UC Berkeley Library.

[1] M. A. Nielsen and I. L. Chuang, *Quantum Computation and Quantum Information: 10th Anniversary Edition* (Cambridge University Press, New York, NY, 2011).

[2] C. Monroe, W. C. Campbell, L.-M. Duan, Z.-X. Gong, A. V. Gorshkov, P. W. Hess, R. Islam, K. Kim, N. M. Linke, G. Pagano, P. Richerme, C. Senko, and N. Y. Yao, Programmable quantum simulations of spin systems with trapped ions, Rev. Mod. Phys. **93**, 025001 (2021).

[3] A. Browaeys and T. Lahaye, Many-body physics with individually controlled Rydberg atoms, Nat. Phys. **16**, 132 (2020).

[4] M. Kjaergaard, M. E. Schwartz, J. Braumüller, P. Krantz, J. I.-J. Wang, S. Gustavsson, and W. D. Oliver, Superconducting qubits: Current state of play, Annu. Rev. Condens. Matter Phys. **11**, 369 (2020).

[5] Y. Li, X. Chen, and M. P. A. Fisher, Quantum Zeno effect and the many-body entanglement transition, Phys. Rev. B **98**, 205136 (2018).

[6] B. Skinner, J. Ruhman, and A. Nahum, Measurement-induced phase transitions in the dynamics of entanglement, Phys. Rev. X **9**, 031009 (2019).

[7] A. C. Potter and R. Vasseur, in *Entanglement in Spin Chains: From Theory to Quantum Technology Applications*, edited by A. Bayat, S. Bose, and H. Johannesson (Springer International Publishing, Cham, 2022), p. 211.

[8] M. P. A. Fisher, V. Khemani, A. Nahum, and S. Vijay, Random quantum circuits, Annu. Rev. Condens. Matter Phys. **14**, 335 (2023).

[9] R. Raussendorf, S. Bravyi, and J. Harrington, Long-range quantum entanglement in noisy cluster states, Phys. Rev. A **71**, 062313 (2005).

[10] L. Piroli, G. Styliaris, and J. I. Cirac, Quantum circuits assisted by local operations and classical communication: Transformations and phases of matter, Phys. Rev. Lett. **127**, 220503 (2021).

[11] N. Tantivasadakarn, R. Thorngren, A. Vishwanath, and R. Verresen, Long-range entanglement from measuring symmetry-protected topological phases, Phys. Rev. X **14** (2), 021040 (2024).

[12] T.-C. Lu, L. A. Lessa, I. H. Kim, and T. H. Hsieh, Measurement as a shortcut to long-range entangled quantum matter, PRX Quantum **3**, 040337 (2022).

[13] G.-Y. Zhu, N. Tantivasadakarn, A. Vishwanath, S. Trebst, and R. Verresen, Nishimori's cat: Stable long-range entanglement from finite-depth unitaries and weak measurements, Phys. Rev. Lett. **131** (20), 200201 (2023).

[14] J. Y. Lee, W. Ji, Z. Bi, and M. P. A. Fisher, Decoding measurement-prepared quantum phases and transitions: From Ising model to gauge theory, and beyond, arXiv:2208.11699.

[15] N. Tantivasadakarn, A. Vishwanath, and R. Verresen, Hierarchy of topological order from finite-depth unitaries, measurement, and feedforward, PRX Quantum **4** (2), 020339 (2023).

[16] M. Foss-Feig, A. Tikku, T.-C. Lu, K. Mayer, M. Iqbal, T. M. Gatterman, J. A. Gerber, K. Gilmore, D. Gresh, A. Hankin, N. Hewitt, C. V. Horst, M. Matheny, T. Mengle, B. Neyenhuis, H. Dreyer, D. Hayes, T. H. Hsieh, and I. H. Kim, Experimental demonstration of the advantage of adaptive quantum circuits, arXiv:2302.03029.

[17] M. Iqbal, N. Tantivasadakarn, T. M. Gatterman, J. A. Gerber, K. Gilmore, D. Gresh, A. Hankin, N. Hewitt, C. V. Horst, M. Matheny, T. Mengle, B. Neyenhuis, A. Vishwanath, M. Foss-Feig, R. Verresen, and H. Dreyer, Topological order from measurements and feed-forward on a trapped ion quantum computer, arXiv:2302.01917.

[18] S. J. Garratt, Z. Weinstein, and E. Altman, Measurements conspire nonlocally to restructure critical quantum states, Phys. Rev. X **13**, 021026 (2023).

[19] J. Y. Lee, C.-M. Jian, and C. Xu, Quantum criticality under decoherence or weak measurement, PRX Quantum **4** (3), 030317 (2023).

[20] Z. Weinstein, R. Sajith, E. Altman, and S. J. Garratt, Nonlocality and entanglement in measured critical quantum Ising chains, Phys. Rev. B **107** (24), 245132 (2023).

[21] Z. Yang, D. Mao, and C.-M. Jian, Entanglement in a one-dimensional critical state after measurements, Phys. Rev. B **108** (16), 165120 (2023).

[22] S. Murciano, P. Sala, Y. Liu, R. S. K. Mong, and J. Alicea, Measurement-altered Ising quantum criticality, Phys. Rev. X **13** (4), 041042 (2023).

[23] X. Sun, H. Yao, and S.-K. Jian, New critical states induced by measurement, arXiv:2301.11337.

[24] J. M. Koh, S.-N. Sun, M. Motta, and A. J. Minnich, Measurement-induced entanglement phase transition on a superconducting quantum processor with mid-circuit readout, Nat. Phys. **19** (9), 1314 (2023).

[25] M. J. Gullans and D. A. Huse, Scalable probes of measurement-induced criticality, Phys. Rev. Lett. **125**, 070606 (2020).

[26] C. Noel, P. Niroula, D. Zhu, A. Risinger, L. Egan, D. Biswas, M. Cetina, A. V. Gorshkov, M. J. Gullans, D. A. Huse, and C. Monroe, Measurement-induced quantum phases realized in a trapped-ion quantum computer, Nat. Phys. **18**, 760 (2022).

[27] H. Dehghani, A. Lavasani, M. Hafezi, *et al.*, Neural-network decoders for measurement induced phase transitions, Nat. Commun. **14**, 2918 (2023).

[28] C. H. Bennett, G. Brassard, C. Crépeau, R. Jozsa, A. Peres, and W. K. Wootters, Teleporting an unknown quantum state via dual classical and Einstein-Podolsky-Rosen channels, Phys. Rev. Lett. **70**, 1895 (1993).

[29] Y. Li and M. P. A. Fisher, Decodable hybrid dynamics of open quantum systems with $\mathbb{Z}_2$ symmetry, Phys. Rev. B **108** (21), 214302 (2023).

[30] F. Barratt, U. Agrawal, A. C. Potter, S. Gopalakrishnan, and R. Vasseur, Transitions in the learnability of global charges from local measurements, Phys. Rev. Lett. **129**, 200602 (2022).

[31] Google Quantum AI and Collaborators, Measurement-induced entanglement and teleportation on a noisy quantum processor, Nature **622**, 481 (2023).

[32] F. Arute, K. Arya, R. Babbush, D. Bacon, J. C. Bardin, R. Barends, R. Biswas, S. Boixo, F. G. Brandao, D. A. Buell, *et al.*, Quantum supremacy using a programmable superconducting processor, Nature **574**, 505 (2019).

[33] Y. Li, Y. Zou, P. Glorioso, E. Altman, and M. P. A. Fisher, Cross entropy benchmark for measurement-induced phase transitions, Phys. Rev. Lett. **130** (22), 220404 (2023).

[34] H.-Y. Huang, R. Kueng, and J. Preskill, Predicting many properties of a quantum system from very few measurements, Nat. Phys. **16**, 1050 (2020).

[35] A. Elben, S. T. Flammia, H.-Y. Huang, R. Kueng, J. Preskill, B. Vermersch, and P. Zoller, The randomized measurement toolbox, Nat. Rev. Phys. **5**, 9 (2023).

[36] J. S. Cotler, D. K. Mark, H.-Y. Huang, F. Hernández, J. Choi, A. L. Shaw, M. Endres, and S. Choi, Emergent quantum state designs from individual many-body wave functions, Phys. Rev. X Quantum **4**, 010311 (2023).

[37] J. Choi, A. L. Shaw, I. S. Madjarov, X. Xie, R. Finkelstein, J. P. Covey, J. S. Cotler, D. K. Mark, H.-Y. Huang, A. Kale, *et al.*, Preparing random states and benchmarking with many-body quantum chaos, Nature **613**, 468 (2023).

[38] W. W. Ho and S. Choi, Exact emergent quantum state designs from quantum chaotic dynamics, Phys. Rev. Lett. **128**, 060601 (2022).

[39] M. Ippoliti and W. W. Ho, Dynamical purification and the emergence of quantum state designs from the projected ensemble, PRX Quantum **4** (3), 030322 (2023).

[40] P. W. Claeys and A. Lamacraft, Emergent quantum state designs and biunitarity in dual-unitary circuit dynamics, Quantum **6**, 738 (2022).

[41] M. McGinley and M. Fava, Shadow tomography from emergent state designs in analog quantum simulators, Phys. Rev. Lett. **131** (16), 160601 (2023).

[42] M. Lucas, L. Piroli, J. De Nardis, and A. De Luca, Generalized deep thermalization for free fermions, Phys. Rev. A **107**, 032215 (2023).
[43] Y. Bao, M. Block, and E. Altman, Finite-time teleportation phase transition in random quantum circuits, Phys. Rev. Lett. **132** (3), 030401 (2024).
[44] C.-J. Lin, W. Ye, Y. Zou, S. Sang, and T. H. Hsieh, Probing sign structure using measurement-induced entanglement, Quantum **7**, 910 (2023).
[45] S. Antonini, G. Bentsen, C. Cao, J. Harper, S.-K. Jian, and B. Swingle, Holographic measurement and bulk teleportation, J. High Energy Phys. **2022**, 124 (2022).
[46] S. Antonini, B. Grado-White, S.-K. Jian, and B. Swingle, Holographic measurement and quantum teleportation in the SYK thermofield double, J. High Energy Phys. **2023**, 1 (2023).
[47] T.-C. Lu, Z. Zhang, S. Vijay, and T. H. Hsieh, Mixed-state long-range order and criticality from measurement and feedback, PRX Quantum **4** (3), 030318 (2023).
[48] P. Sierant, G. Chiriacò, F. M. Surace, S. Sharma, X. Turkeshi, M. Dalmonte, R. Fazio, and G. Pagano, Dissipative Floquet dynamics: From steady state to measurement induced criticality in trapped-ion chains, Quantum **6**, 638 (2022).
[49] M. McGinley, S. Roy, and S. A. Parameswaran, Absolutely stable spatiotemporal order in noisy quantum systems, Phys. Rev. Lett. **129**, 090404 (2022).
[50] A. J. Friedman, O. Hart, and R. Nandkishore, Measurement-induced phases of matter require feedback, PRX Quantum **4** (4), 040309 (2023).
[51] T. Iadecola, S. Ganeshan, J. H. Pixley, and J. H. Wilson, Dynamical entanglement transition in the probabilistic control of chaos, arXiv:2207.12415.
[52] M. Buchhold, T. Müller, and S. Diehl, Revealing measurement-induced phase transitions by pre-selection, arXiv:2208.10506.
[53] N. O'Dea, A. Morningstar, S. Gopalakrishnan, and V. Khemani, Entanglement and absorbing-state transitions in interactive quantum dynamics, Phys. Rev. B **109** (2), L020304 (2024).
[54] V. Ravindranath, Y. Han, Z.-C. Yang, and X. Chen, Entanglement steering in adaptive circuits with feedback, Phys. Rev. B **108** (4), L041103 (2023).
[55] L. Piroli, Y. Li, R. Vasseur, and A. Nahum, Triviality of quantum trajectories close to a directed percolation transition, Phys. Rev. B **107** (22), 224303 (2023).
[56] P. Sierant and X. Turkeshi, Controlling entanglement at absorbing state phase transitions in random circuits, Phys. Rev. Lett. **130**, 120402 (2023).
[57] G. Lindblad, Completely positive maps and entropy inequalities, Commun. Math. Phys. **40**, 147 (1975).
[58] Z. Webb, The Clifford group forms a unitary 3-design, Quantum Inf. Comput. **16**, 1379 (2016).
[59] H. Zhu, Multiqubit Clifford groups are unitary 3-designs, Phys. Rev. A **96**, 062336 (2017).
[60] A. Zabalo, M. J. Gullans, J. H. Wilson, S. Gopalakrishnan, D. A. Huse, and J. H. Pixley, Critical properties of the measurement-induced transition in random quantum circuits, Phys. Rev. B **101**, 060301 (2020).
[61] U. Schollwöck, The density-matrix renormalization group in the age of matrix product states, Ann. Phys. (NY) **326**, 96 (2011).
[62] L. Tagliacozzo, T. R. de Oliveira, S. Iblisdir, and J. I. Latorre, Scaling of entanglement support for matrix product states, Phys. Rev. B **78**, 024410 (2008).
[63] F. Pollmann, S. Mukerjee, A. M. Turner, and J. E. Moore, Theory of finite-entanglement scaling at one-dimensional quantum critical points, Phys. Rev. Lett. **102**, 255701 (2009).
[64] B. Pirvu, G. Vidal, F. Verstraete, and L. Tagliacozzo, Matrix product states for critical spin chains: Finite-size versus finite-entanglement scaling, Phys. Rev. B **86**, 075117 (2012).
[65] Y. Bao, S. Choi, and E. Altman, Theory of the phase transition in random unitary circuits with measurements, Phys. Rev. B **101**, 104301 (2020).
[66] C.-M. Jian, Y.-Z. You, R. Vasseur, and A. W. W. Ludwig, Measurement-induced criticality in random quantum circuits, Phys. Rev. B **101**, 104302 (2020).
[67] G. Vidal and R. F. Werner, Computable measure of entanglement, Phys. Rev. A **65**, 032314 (2002).
[68] S. Boixo, S. V. Isakov, V. N. Smelyanskiy, R. Babbush, N. Ding, Z. Jiang, M. J. Bremner, J. M. Martinis, and H. Neven, Characterizing quantum supremacy in near-term devices, Nat. Phys. **14**, 595 (2018).
[69] A. Elben, B. Vermersch, C. F. Roos, and P. Zoller, Statistical correlations between locally randomized measurements: A toolbox for probing entanglement in many-body quantum states, Phys. Rev. A **99**, 052323 (2019).
[70] B. Vermersch, A. Rath, B. Sundar, C. Branciard, J. Preskill, and A. Elben, Enhanced estimation of quantum properties with common randomized measurements, PRX Quantum **5** (1), 010352 (2024).
[71] T. Brydges, A. Elben, P. Jurcevic, B. Vermersch, C. Maier, B. P. Lanyon, P. Zoller, R. Blatt, and C. F. Roos, Probing Rényi entanglement entropy via randomized measurements, Science **364**, 260 (2019).
[72] M. K. Joshi, A. Elben, B. Vermersch, T. Brydges, C. Maier, P. Zoller, R. Blatt, and C. F. Roos, Quantum information scrambling in a trapped-ion quantum simulator with tunable range interactions, Phys. Rev. Lett. **124**, 240505 (2020).
[73] D. Zhu, Z.-P. Cian, C. Noel, A. Risinger, D. Biswas, L. Egan, Y. Zhu, A. M. Green, C. H. Alderete, N. H. Nguyen, *et al.*, Cross-platform comparison of arbitrary quantum states, Nat. Commun. **13**, 6620 (2022).
[74] J. C. Napp, R. L. La Placa, A. M. Dalzell, F. G. S. L. Brandão, and A. W. Harrow, Efficient classical simulation of random shallow 2D quantum circuits, Phys. Rev. X **12**, 021021 (2022).
[75] S. Aaronson, Quantum computing, postselection, and probabilistic polynomial-time, Proc. R. Soc. A **461**, 3473 (2005).
[76] M. J. Bremner, R. Jozsa, and D. J. Shepherd, Classical simulation of commuting quantum computations implies collapse of the polynomial hierarchy, Proc. R. Soc. A **467**, 459 (2011).